Lab on a Chip

RSC Publishing

PAPER

View Article Online
View Journal | View Issue

Cite this: *Lab Chip*, 2013, **13**, 4190

Ultrasensitive microfluidic solid-phase ELISA using an actuatable microwell-patterned PDMS chip†

Tanyu Wang,[a] Mohan Zhang,[a] Dakota D. Dreher[a] and Yong Zeng*[abc]

Received 28th June 2013,
Accepted 6th August 2013

DOI: 10.1039/c3lc50783a

www.rsc.org/loc

Quantitative detection of low abundance proteins is of significant interest for biological and clinical applications. Here we report an integrated microfluidic solid-phase ELISA platform for rapid and ultrasensitive detection of proteins with a wide dynamic range. Compared to the existing microfluidic devices that perform affinity capture and enzyme-based optical detection in a constant channel volume, the key novelty of our design is two-fold. First, our system integrates a microwell-patterned assay chamber that can be pneumatically actuated to significantly reduce the volume of chemifluorescent reaction, markedly improving the sensitivity and speed of ELISA. Second, monolithic integration of on-chip pumps and the actuatable assay chamber allow programmable fluid delivery and effective mixing for rapid and sensitive immunoassays. Ultrasensitive microfluidic ELISA was demonstrated for insulin-like growth factor 1 receptor (IGF-1*R*) across at least five orders of magnitude with an extremely low detection limit of 21.8 aM. The microwell-based solid-phase ELISA strategy provides an expandable platform for developing the next-generation microfluidic immunoassay systems that integrate and automate digital and analog measurements to further improve the sensitivity, dynamic ranges, and reproducibility of proteomic analysis.

Introduction

Quantitative detection of low abundance proteins is of significant interest for biological and clinical applications. For instance, ultrahigh sensitivity is imperative for single cell proteomic analysis to characterize the phenotypic heterogeneity of cells and to interrogate the underlying cellular regulation networks and signaling pathways.[1–3] Many protein biomarkers present in the concentration range of 10^{-16} to 10^{-12} M in biofluids such as cerebral spinal fluid from Alzheimer's disease[4] and blood samples from cancer patients.[5] Therefore, significant efforts have been continuously invested to develop a variety of technologies for ultrasensitive protein detection, including nanoparticle-based bio-barcode,[6] immuno-PCR,[7] electrochemical biosensors,[8] microfluidic immunoassay[9] and single-molecule detection methods.[10,11]

Enzyme-linked immunosorbent assay (ELISA) has been the workhorse tool for protein detection in research and clinical laboratories. While powerful and flexible, the standard ELISA format (*i.e.* micro-titer plate) suffers from a number of limitations. Microplate ELISA requires large volumes of reagents (50 to 100 μL each step) and long incubation times (up to two days).[12] Antibodies can be costly and vary in affinity from batch to batch,[13] which can be a practical constraint for high-throughput screening. In addition, the assay performance heavily relies on manual practice and the competence of the operator, which has been reported as a major source of analysis variance by a comprehensive study organized by the Human Proteome Organization (HUPO).[14] Microfluidics is uniquely positioned to overcome these limitations, due to its ability to precisely process nanoliter volumes or less, improve bioassay performance, and to enable large-scale integration and automation.[15] A vast number of microfluidic systems have been developed for the miniaturization and integration of ELISA and other types of immunoassays.[9,12,16–19] These assays typically perform solid-phase immunoassays on microchannel surface,[20–22] bead,[23,24] or hydrogel matrices.[13,25] Although the microfluidic format has considerably improved the performance of immunoassays, the sensitivity of many of these assays is still limited from femto- to picomolar (pg mL^{-1} to ng mL^{-1}).[7] Digital immunoassays have recently emerged as a powerful technology for quantitative detection of extremely low abundance proteins.[10,26–28] These assays use femtoliter (fL) microwells[10] or droplets[28] to compartmentalize individual target molecules for single-molecule chemifluorescence detection. However, current digital ELISA methods suffer from limited dynamic range[27] and rely on manual, off-chip operations to capture targets on beads.[26,28] Therefore, there

[a]*Department of Chemistry, University of Kansas, Lawrence, KS 66045, United States. E-mail: yongz@ku.edu; Fax: +1 (785) 864-5396; Tel: +1 (785) 864-8105*
[b]*Ralph N Adams Institute for Bioanalytical Chemistry, University of Kansas, Lawrence, KS 66045, United States*
[c]*Bioengineering Graduate Program, University of Kansas, Lawrence, KS 66045, United States*

† Electronic supplementary information (ESI) available. See DOI: 10.1039/c3lc50783a

is a pressing need of new technologies to further improve the analytical performance of immunoassays because many biomarkers are expressed across an extremely broad concentration range and it is believed that most serum proteins are, in fact, currently undetectable.[10,11,29,30]

Here we develop an integrated microfluidic solid-phase ELISA platform that enables rapid and ultrasensitive detection of proteins with a wide dynamic range. Traditional methods usually perform antibody-capture and enzyme-based optical detection in a constant channel volume. In contrast, our system integrates a microwell-patterned assay chamber that can be pneumatically actuated to significantly reduce the volume of chemifluorescent reaction, markedly improving the sensitivity and speed of the on-chip ELISA. Monolithic integration of the micropumps and the actuatable assay chamber allows programmable fluid delivery and effective mixing to further enhance the assay performance.[18,31,32] Moreover, the adaptation of the fL microwell pattern in our design offers structural compatibility with the digital detection which would allow us to develop new automated microfluidic immunoassays that integrate both digital and analog measurements. Using this novel approach, we have demonstrated quantitative and sensitive detection of a model protein biomarker, insulin-like growth factor 1 receptor (IGF-1R). IGF-1R is a cell–surface tyrosine kinase receptor that plays a predominating role in IGF-1 signaling pathways. IGF-1R is highly implicated in tumor transformation, invasion and metastasis in a variety of cancers including breast cancer, prostate cancer, and lung cancer.[33–35] IGF-1R might be a biomarker for treatment efficacy[35] and drug resistance.[36] Evaluating the potential of IGF-1R for targeted anti-cancer therapy is of particular interest in current cancer research.[33–35] Our method affords quantitative detection of IGF-1R across at least five orders of magnitude with a limit of detection (LOD) of 3.5 fg mL^{-1} (21.8 aM). Compared with the commercial ELISA kits (see Table S1, ESI†), our method increases the detection sensitivity by at least three orders of magnitude and reduces the assay time and reagent/sample consumption by about one order of magnitude (Table 1). The pneumatic actuator-based design is scalable for large-scale microfluidic integration[37] and could be adapted for high throughput, multiplexed and quantitative measurement of low-level biomarkers for early diagnosis of diseases, assessment of treatment efficacy and monitoring of disease relapse.

Table 1 Typical protocol of microfluidic femtoliter array compared to standard 96-well plate ELISA[12]

Assay Reagents	Microfluidic ELISA		96-well Plate ELISA	
	Volume	Duration	Volume/well	Duration
Capture antibody	10 μL	15 min	100 μL	Overnight
Washing buffer	30 μL	15 min	300 μL × 5	~10 min
Blocking buffer	—	—	200 μL	1.5 h
Washing buffer	—	—	300 μL × 5	~10 min
Antigen	10 μL	15 min	100 μL	2 h
Washing buffer	30 μL	15 min	300 μL × 5	~10 min
Detection antibody	10 μL	15 min	100 μL	1 h
Washing buffer	30 μL	15 min	300 μL × 5	~10 min
Reporter enzyme	10 μL	15 min	100 μL	1 h
Washing buffer	30 μL	15 min	300 μL × 5	~10 min
Substrate	10 μL	5 min	100 μL	15 min
Total time	125 min		Overnight + 6.5 h	

Experimental

Reagents and materials

All solutions were prepared with deionized water (18.2 MΩ-cm, Thermo Scientific). The following reagents were used as received: trimethyl chlorosilane (Thermo Scientific), 1× phosphate-buffered saline solution (1× PBS) (⩾98.5, Mediatech, Inc.), SuperBlock T20 blocking buffer (PBST) (Thermo Scientific), 3-aminopropyl triethoxysilane (APTES) (99%; Sigma-Aldrich), fluorescein di-β-D-galactopyranoside (FDG) (Invitrogen), biotin labeled β-galactosidase (BβG) (Sigma-Aldrich), streptavidin (SA)(Sigma-Aldrich), streptavidin β-galactosidase conjugate (SβG) (Invitrogen), 2-propanol (IPA) (⩾99.5%; Sigma-Aldrich), ethanol (100%, Decon Laboratories Inc.), human IGF-1R antibody (Ab1) (R&D Systems), human IGF-1R biotinylated antibody (B-Ab2) (R&D Systems), recombinant human IGF-1 receptor (IGF-1*R*) (>95%, R&D Systems). PBS working solution (PBSW) at pH 7.4 was freshly prepared in house, containing 0.5 mM DL-dithiothreitol solution (Sigma-Aldrich), 2 mM $MgCl_2$ (Fluka Analytical), and 5% bovine serum albumin (BSA) (Sigma-Aldrich).

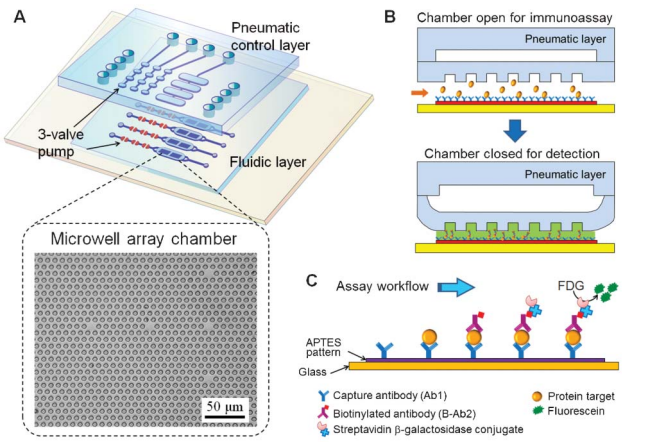

Fig. 1 Integrated microfluidic ELISA. (A) Schematic of the design of a three-layer PDMS/glass chip that integrates a three-valve pump and an assay chamber containing an array of femtoliter microwells (inset). The chip has four parallel units controlled by a single pneumatic control circuit for simultaneous protein assays. (B) Pneumatic actuation of the assay chamber for solid-phase immunoassay (upper) and chemifluorescence detection (bottom). Under the low pressure (30–70 kPa) applied to the pneumatic chamber, the microwell array membrane can be quickly deformed to create an array of femtoliter detection volumes interconnected by a thin layer of liquid. (C) Schematic of the procedure of the sandwich immunoassay on the APTES coated substrate surface inside the microfluidic chamber. β-gal was used as the reporter enzyme to convert non-fluorescent fluorescein di-β-D-galactopyranoside (FDG) to fluorescein products for fluorescence detection.

Microfabrication and device assembly

Standard photo-lithography and soft-lithography were used to prepare the SU-8 molds on silicon wafers and polydimethylsiloxane (PDMS) chips as sketched in Fig. 1A. The Si mold for the pneumatic layer was fabricated using SU-8 2050 (MicroChem) with a final thickness of ~30 μm, following the recommended procedure by the manufacturer. The mold for the fluidic layer was fabricated by the two-step lithography. Briefly, the 30 μm thick channel features was first patterned with SU-8 2050 photoresist following the same procedure as above. The micropost array was patterned on top of the first layer by spin-coating SU-8 2010 at 4500 rpm for 60 s. The wafer was prebaked at 65 °C for 2 min and at 95 °C for 4 min, and exposed for 9 s for total exposure energy of 110 mJ cm^{-2}. The wafer was then post-baked at 65 °C for 1 min and at 95 °C for 4 min, followed by a 2 min development and hard-baking at 165 °C for 30 min. Before making PDMS chips, all Si molds were treated with trimethylchlorosilane by gas phase silanization under vacuum for 4 h.

For the pneumatic layer, 30 g PDMS (Dow Corning, USA) mixture at a 5 (base material) : 1 (curing agent) ratio was poured on the mold and cured in the oven at 70 °C for 40 min. PDMS slab was then peeled off from the mold and cut into rectangular pieces. Access holes were punched in the PDMS replica of the pneumatic layer for pneumatic connections. Meanwhile, 5 g PDMS mixed at a ratio of 20 : 1 was spin-coated over the mold at 300 rpm for 30 s twice and cured on a 70 °C hotplate for 30 min to make the fluidic membrane layer. The pneumatic layer was then manually aligned under a stereomicroscope and permanently bonded with the bottom fluidic layer by baking in the 70 °C oven overnight. The assembly was then removed from the mold and the holes were punched for fluid access.

The glass substrate was patterned with APTES through silanization to enhance the adsorption of capture antibody within the area of the assay chamber (Fig. 1B). To this end, a glass slide (76.2 mm × 25.4 mm, Fisher Scientific) was first cleaned with freshly prepared piranha solution (3 : 1 mixture of concentrated H_2SO_4 with H_2O_2) for 15 min, rinsed thoroughly with deionized water, and dehydrated by baking on a 95 °C hotplate for 30 min. Hot piranha is extremely dangerous and should be handled with appropriate personal protection in a fumehood free of organic chemicals. The specific area of the glass was then patterned by 5% APTES aqueous solution at 95 °C for 1 h using a microchannel molding method.[38] The glass was washed with ethanol and DI water to remove unreacted APTES. PDMS device was ethanol cleaned and treated with UV Ozone (UVO-Cleaner® 42, Jelight Company Inc.) for 2 min. The cleaned PDMS assembly was aligned and reversibly bonded with the APTES patterned glass.

Microfluidic immunoassays

The monolithic diaphragm valves and assay chamber were actuated by a homemade solenoid controller interfaced with a computer *via* a LabVIEW program. A 4-step pumping sequence with various pulse time and closing pressure was used with the vacuum fixed at −87 kPa.[39] Fig. 1C details the workflow of the sandwich ELISA performed on the surface of the microfluidic chamber. The capture antibody (Ab1) was first flowed through the assay chamber where the surface was silanized with APTES to enhance the immobilization of Ab1 through electrostatic interaction between the negatively charged antibodies and the positively charged amine group of APTES.[22] The antigen can be captured, recognized by the biotinylated detection antibody (B-Ab2), and quantified using β-galactosidase (β-gal) as the reporter enzyme for chemifluorescence detection. Both bright field and fluorescence images were taken using a Zeiss Axiovert A1 inverted fluorescence microscope equipped with a LED excitation light source (Thorlabs, Newton, NJ). The digital images were processed and analyzed using ImageJ (NIH, http://rsbweb.nih.gov/ij/) to measure the fluorescence intensity.

For the BβG assay, the channel surface is first coated with 100 μg mL^{-1} of streptavidin (10 μL) in PBS buffer and then blocked by 5% BSA in PBSW. After washing with 10 μL PBSW buffer, 10 μL BβG of various concentrations (0.005 to 50 ng mL^{-1}) were pumped through the assay chambers using the settings described in the main text. As a final step, 500 μM of fluorescein di-β-d-galactopyranoside (FDG) was filled in the chip by on-chip pumping and the assay chambers were pushed down with a 65 kPa pressure applied to the pneumatic channel immediately. The microscope was adjusted to focus on the microwells and the fluorescence images were taken 15 min after the closure of the chamber with an exposure time of 2500 ms. In the immunoassay for IGF-1R, 8 μg mL^{-1} of Ab1 in PBS was first coated on the channel surface which was then blocked and washed by 30 μL of PBST buffer. To generate the standard curve, various concentrations of human IGF-1R (10 μL) in PBS buffer with 5% BSA were pumped through the assay chambers and washing with 30 μL of PBST. 0.1 μg mL^{-1} of B-Ab2 (10 μL) was then loaded to label the surface immobilized target proteins. Unbound B-Ab2 was washed off with 30 μL of PBST and then 0.2 μg mL^{-1} of SβG (10 μL) in PBSW was loaded into the assay chambers. After the last washing step with 30 μL of PBST, the assay chambers will be filled with 0.5 to 2.5 mM FDG and immediately pressed down by a 65 KPa pressure applied to the pneumatic channel. The microscope was adjusted to focus on the microwells and the fluorescence images were taken using an exposure time of 1500–2500 ms. Since the chip has four parallel units controlled by a single pneumatic control circuit, up to four assays were carried out simultaneously.

Results and discussion

Microfluidic design

A number of microfluidic devices have been demonstrated for ELISA based on the microchannel surface[13,40–42] or beads.[19,43–45] In these microsystems, the affinity capture and enzyme-based detection were performed in the same volume. It has been shown that reducing detection volume can significantly enhance the sensitivity of enzymatically fluorogenic detection.[10] However, simply reducing channel sizes would dramatically reduce the volumetric flow rate of sample and assay reagents, leading to excessively long analysis time.

Therefore, the key concept of our microfluidic design is to integrate a volume adjustable assay chamber to enable fast surface-based immuno-capture and ultrasensitive chemifluorescence detection. We have developed a prototype device, which is a three-layer PDMS/glass assembly, as illustrated in Fig. 1A. It contains four parallel assay units which are actuated by one pneumatic control circuit fabricated on the top PDMS layer. Each unit integrates an on-chip pump composed of three lifting gate microvalves[46] and an immunoassay chamber, both fabricated on a ~300 μm thick PDMS layer. An array of microwells was also fabricated on the ceiling of the chamber to improve the optical detection (Fig. 1A, bottom), as discussed below. The dimensions of the wells were ~4.2 μm in diameter and ~6 μm in height, giving a volume of ~83 fL, with a center-to-center distance of 10 μm. As sketched in Fig. 1B, the microwell-patterned membrane can be pneumatically actuated to open up the assay chamber for rapid flow-through sandwich immunoassay and to close for conducting chemi-fluorescence detection in a greatly reduced volume. Such volume reduction is expected to accelerate the enzymatic reaction and enhance the detection sensitivity due to greatly increased effective concentrations of the captured targets and the fluorescent products of the enzymatic reaction.

It is important to note that our readout method is fundamentally different from a digital immunoassay, although both use the microwell structure. In a digital immunoassay, the microwell structure is used to partition and isolate single molecules for binary counting of the molecules.[10,47] Our microfluidic design stems from the observation that when a PDMS membrane is pneumatically pressed against the hydrophilic glass substrate under relatively low pressure (30–80 kPa), a thin layer of aqueous liquid can be retained in between. We demonstrated that this phenomenon also occurs to the PDMS membrane patterned with a high-density fL microwell array, by comparing to sealing a microwell device on the hydrophobic PDMS surface (Fig. S1, ESI†). Trapping aqueous solution at the PDMS/glass interface can be attributed to the hydrophilic glass surface, BSA absorbed on the surface, and the surfactant and highly concentrated BSA in the buffer. The microwell structure was adapted in our method not only to substantially enhance the sensitivity of fluorescent detection, as discussed in Fig. 2, but also to confer the structural compatibility with the digital readout techniques, which would allow us to develop the next-generation microfluidic platforms that integrate both digital and analog immunoassays.

To assess the microwell-assisted microfluidic chemifluorescence detection, a streptavidin-biotin assay was implemented to detect biotinylated β-galactosidase (BβG), as drawn in Fig. 2A. A typical fluorescence image was presented in Fig. 2B for the BβG concentrations of 0 and 5 ng mL^{-1}, respectively, showing the successful detection of BβG. Fluorescence intensity profiles across an array of wells were measured for a serial 10-fold dilution of BβG, which shows fairly constant fluorescence intensity across the microwells (Fig. 2C). It was also observed that the signal levels in the microwells and the flat area outside the wells increase with the target concentration. Both signals exhibit a linear response when plotted as a logarithmic function of concentration, as manifested in Fig. 2D, which further confirms the formation of a thin layer

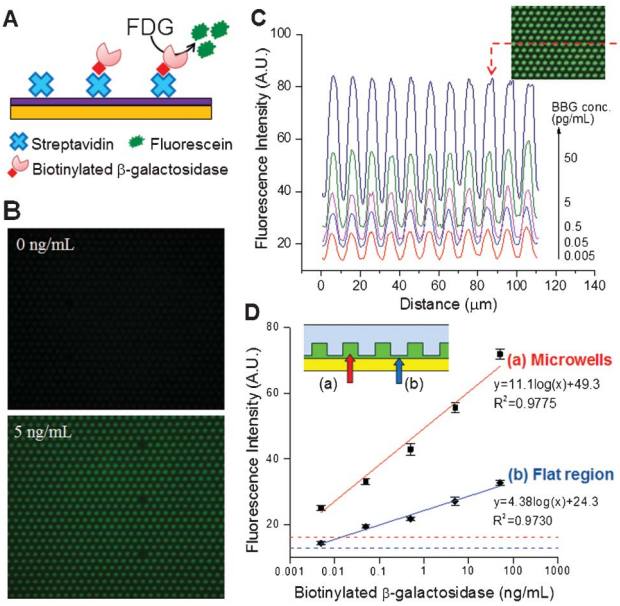

Fig. 2 Enhanced chemifluorescence detection using the actuatable microwell-patterned device. (A) Schematic of the streptavidin-biotin assay, in which biotinylated β-galactosidase (BβG) is captured by streptavidin immobilized on the APTES coated surface and detected by measuring fluorescein converted from the non-fluorescent substrate FDG by BβG. (B) Two typical false-color fluorescence images obtained at the BβG concentrations of 0 and 5 ng mL^{-1}, respectively. (C) Typical intensity profiles measured across an array of wells in the fluorescence images taken for a serial 10-fold dilution of BβG (5 pg mL^{-1} to 50 ng mL^{-1}). (D) Fluorescence signals measured in the microwells (a) and the flat region outside the wells (b), as indicated in the inset, were plotted to determine the detection sensitivity. The microwell-based signal measurement offers a 2.54-fold higher sensitivity than that of the flat region. Dashed lines indicate the value of blank signal plus three standard deviations. Error bars indicate standard deviations of three replicate assays (n = 3).

of liquid between the membrane and the glass substrate. Small variation observed among the experiment replicates suggests that the formation of the aqueous thin layer is uniform and reproducible. The analytical sensitivity was determined from the calibration curves in Fig. 2D, which shows a 2.54-fold increase for the microwell-assisted detection. Such improvement is presumably due to the much larger optical depth of the microwells as opposed to the thin liquid layer trapped between the PDMS and glass surfaces. Thus, our results underscore the importance of fL microwell structure in the actuatable assay chamber design to enhance the sensitivity of fluorescence detection. Another advantage of the microwell structure over the thin-layer only structure is that it offers higher substrate capacity for enzymatic chemifluorescence detection, which is important to achieving quantitative detection over a wide dynamic range, as further discussed below.

Microfluidic pumping

An important factor in solid-phase immunoassay is effective affinity capture of protein targets. Using our device, we are able to program on-chip pumping to control the sequential fluidic delivery for the sandwich immunoassay using β-gal as

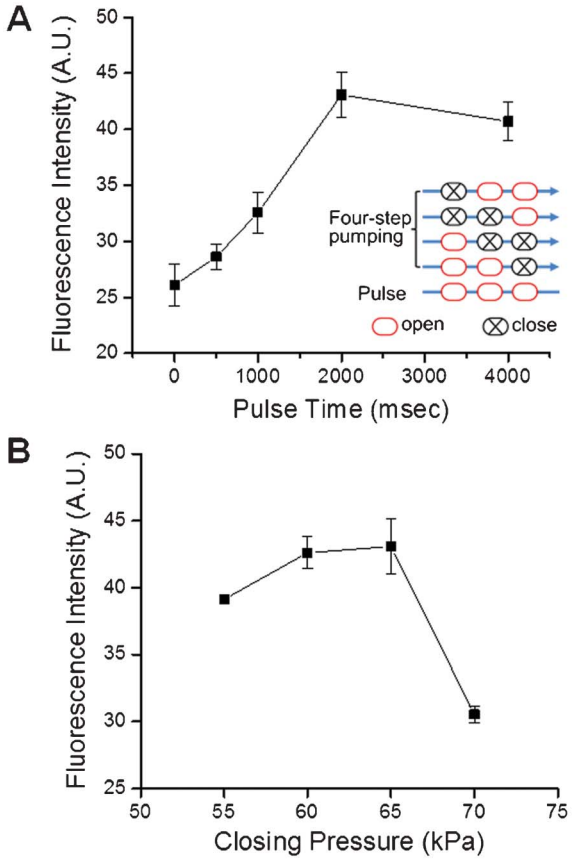

Fig. 3 Optimization of on-chip pumping using the BβG assay. (A) Effects of the stop-flow pumping method on the performance of target capture. A four-step pumping sequence was used with the actuation time for each step fixed at 500 ms and the pulse time varied from 0 to 4 s (inset). (B) Effects of valve closing pressure on the performance of target capture. The vacuum applied to the valves was fixed at −87 kPa. Error bars indicate standard deviations of three replicate assays (n = 3).

the reporter enzyme (Fig. 1C). Thus pneumatic pumping settings should have direct impact on the performance of the on-chip ELISA. Using the BβG assay, we optimized the microfluidic pumping parameters, as summarized in Fig. 3. Since β-gal from E. coli used here is a fairly large molecule with a molecular weight of 540 kDa, the optimal pumping settings obtained here should be applicable for efficient capture of many protein biomarkers, including recombinant human IGF-1R (~160 kDa). We first investigated the effect of a stop-flow pumping method on protein capture efficiency (Fig. 3A). A four-step pumping sequence[48] was consistently used with the actuation time for each step set to 500 ms to ensure full closure of the valves under the pressure range applied.[46] The pulse time between each cycle was then adjusted to control the incubation time in the assay chamber (Fig. 3A inset). It is shown that the stop-flow method yields higher signal levels than the continuous pumping (*i.e.*, pulse time = 0 s) and exhibits a maximum fluorescence signal at the pulse duration of 2 s. This observation is qualitatively consistent with the previous theoretical study which showed that the stop-flow method results in more efficient surface affinity capture than the continuous flow process, especially with slow binding kinetics, low target concentrations or short capture channels.[49]

Flow rate is a critical parameter that affects the kinetics of heterogeneous immunoassay inside microchannels. For instance, due to the large surface-to-volume ratio, depletion of analyte in the assay chamber leads to low capture efficiency.[49] Fast flow can replenish the analyte to maintain the binding rate, but will also reduce the time for analyte molecules to diffuse to the surface and to interact with the immobilized capture probe. Therefore, we examined the effects of closing pressure for pump actuation because it directly controls the flow rate of liquid generated by the on-chip pumping. As shown in Fig. 3B, the obtained signal intensity was fairly consistent with closing pressure lower than 65 kPa while decreased by 29% at 70 kPa. This behavior agrees well with the numerical and experimental results reported by Parsa *et al.*, which can be mainly attributed to the limited amount of analyte that diffuse onto the active surface at high flow rates.[50] Our observation suggests that the immunoassay be operated at the closing pressure of 65 kPa which yields an optimal flow rate (~0.7 μL min^{-1} on average) to achieve the maximum signal with the shortest possible time. Furthermore, the chamber membrane was also periodically actuated, which generates convective mixing inside the assay chamber to enhance immunosorption kinetics and thus improve the analytical performance of solid-phase immunoassay.[32,51] Compared to commonly used syringe pumps, integration of monolithic micropump affords convenient and precise programing of fluid delivery as well as the potential for full automation of on-chip bioanalysis.[22,51]

Ultrasensitive microfluidic ELISA

We next sought to implement and characterize our microfluidic ELISA technology for biomarker detection by using human IGF-1R as the model target. IGF-1R is a cell-surface tyrosine kinase receptor that plays a predominating role in the IGF-1 signaling pathways and is clinically implicated in a variety of cancers, such as breast cancer, prostate cancer, and lung cancer.[33–35] IGF-1R might be a biomarker for treatment efficacy,[35] prognosis,[52] and drug resistance.[36] Developing sensitive and quantitative IGF-1R assays is of great interest for cancer research, such as single cell mapping of signaling networks,[53] as well as for clinical diagnostics and therapeutics.[36]

To maximize the signal to noise ratio, we first optimized the assay conditions to reduce the background arising from physical adsorption of proteins on PDMS surface and non-specific protein interactions. A commercial SuperBlock blocking buffer in PBS with 0.05% Tween-20 surfactant (PBST) was used for effective blocking of PDMS surface and unoccupied sites. We investigated various concentrations of the biotinylated detection antibody (B-Ab2) and washing volumes, as seen in Fig. S2 (Supporting Information†). The combination of 0.1 mg mL^{-1} B-Ab2 with 30 μL PBST washing yielded a dramatically reduced background level without excessively extending the assay time. In these experiments, 0.2 μg mL^{-1} of SβG was adapted according to previous studies.[54] All these established assay steps are summarized in Table 1, which

shows remarkable savings in reagent and sample consumption and analysis time in comparison to the typical procedure of conventional 96-well plate ELISA.

A factor that limits the quantitative performance of microscale immunoassays is the depletion of substrate in enzymatic conversion.[27] We studied the conversion of FDG by immobilized β-gal over time under three different FDG concentrations in order to determine the substrate concentration and reaction time that maximize the S/N ratio while avoiding significant substrate depletion. Fig. S3 (Supporting Information†) plots the average fluorescence intensity of wells acquired every 100 s for the FDG concentrations of 500 μM and 1 mM, which are much higher than the Michaelis constant (18 μM) for FDG hydrolysis by β-gal in solution.[55,56] The IGF-1F concentration was fixed at 0.1 ng mL^{-1}, which is at the high end of the concentration range that we tested. The first measurement (*i.e.*, t = 0 s in Fig. S3, ESI†) was made approximately 30 s after the closure of the assay chamber which was the time required for manual focusing using the current imaging setup. As expected by the Michaelis–Menten kinetics, the signal obtained for both FDG concentrations exhibits a roughly linear increase along with time and reaches plateau after t = ~600 s. We also tested a very high FDG concentration of 2.5 mM and observed noticeably higher background for the negative control ([IGF-1R] = 0 ng mL^{-1}). Therefore, we have chosen the incubation time of 500 s and the FDG concentration of 1 mM to achieve broad dynamic range and high sensitivity of our microfluidic IGF-1R assay.

Using the conditions optimized above, we calibrated the microfluidic ELISA combined with the microwell assisted chemifluorescence detection for quantitative detection of IGF-1R protein. The fluorescence images acquired for different concentration standards were displayed in Fig. 4A, which show a very low background level for the blank control and increasing fluorescence intensity along with the IGF-1R concentration. The fluorescent signal in the microwells appears to be fairly uniform even at low average concentrations (<1 copy per well), which can be attributed to the diffusion of fluorescein across the interconnected wells. We estimated that a fluorescein molecule can diffuse over ~520 μm (*i.e.*, 52 microwells) in PBS during the 500 s incubation time using a diffusion coefficient of 2.6 × 10^{-6} cm^2 s^{-1}.[57] Such large diffusion length should lead to the uniform distribution of fluorescein over the thin liquid layer, which is also supported by the experimental comparison between analog and digital β-Gal detection at an average concentration of 0.09 copies per well in Fig. S1, ESI.† The averaged fluorescence intensity in the microwells was plotted as a logarithmic function of IGF-1R concentration (Fig. 4B). It is demonstrated that our microfluidic ELISA system enables quantitative detection of IGF-1R over an extensive dynamic range of 10 fg mL^{-1} to 1 ng mL^{-1} with a remarkably low LOD of 3.5 fg mL^{-1} (21.8 aM) calculated from the value of blank signal plus three standard deviations. Such low detection limit offered by the novel microfluidic ELISA is comparable with that of some ultrasensitive biosensors, such as nanoparticle-based bio-bar codes (30 aM PSA without PCR amplification),[6] magneto-nanosensor (50 aM carcinoembryonic antigen),[58] whispering-gallery microcavity (5 aM interleukin-2),[11] and

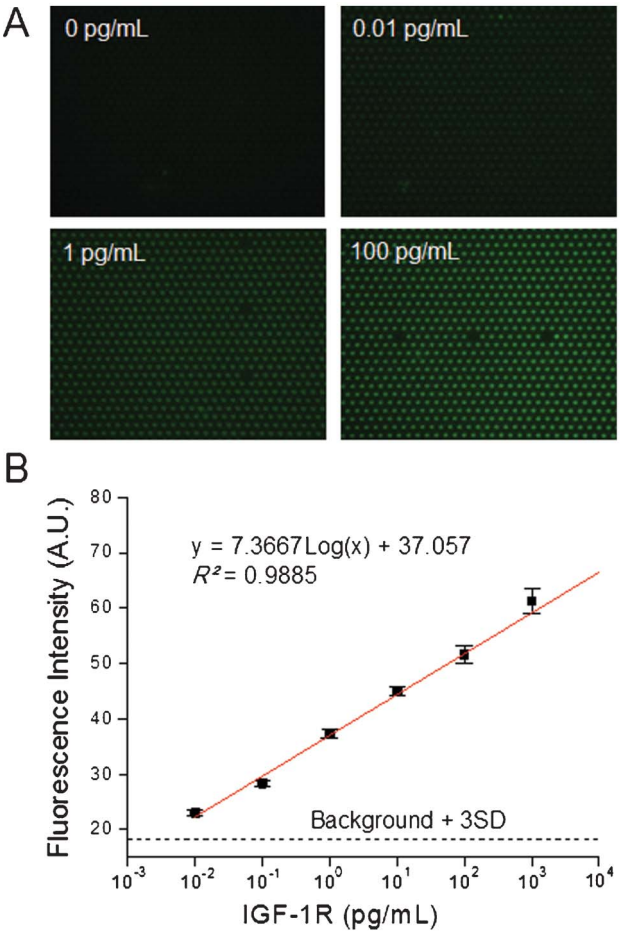

Fig. 4 Ultrasensitive microfluidic ELISA for IGF-1R protein. (A) Typical fluorescence images (false color) showing a very low background level for the blank control and increasing signal intensity with the IGF-1R concentration. Chemifluorescence detection conditions: [SβG] = 0.2 μg mL^{-1}, [FDG] = 1 mM, incubation time = 500 s and exposure time = 2.5 s. (B) Semi-logarithmic calibration curve of microfluidic IGF-1R ELISA under the same conditions above. The averaged signal intensity in the microwells was plotted as a logarithmic function of IGF-1R concentrations. Quantitative detection of IGF-1R was achieved over a dynamic range of 10 fg mL^{-1} to 1 ng mL^{-1} with a theoretical LOD of 3.5 fg mL^{-1} (21.8 aM) calculated from the value of blank signal plus three standard deviations. Error bars are standard deviations of two replicate experiments.

microfluidic digital ELISA (0.011 pg mL^{-1} PSA).[26] In addition, our microfluidic ELISA outperforms all the commercial ELISA kits in terms of sensitivity and detection range by orders of magnitude (Supporting Information,† Table S1).

Ultrasmall-volume confinement provides a powerful means to markedly enhance the detection sensitivity of chemical and biochemical analysis, but is limited in dynamic range.[27] Rissin *et al.* have demonstrated digital ELISA by confining single-molecule fluorogenic reaction in individual fL microwell reactors.[10] To extend the dynamic range of digital ELISA, the authors also reported a hybrid approach that combines both the single-molecule counting (digital) and the measurement of averaged signal yielded by the singulated ensembles of molecules confined in the individual fL reactors (analog).[27]

Substrate depletion was found to be a limiting factor at high concentration because a large number of enzyme molecules confined in a fL volume can quickly consume the substrate such that the turnover rate decreases dramatically over time. As a result, the improvement of dynamic range was limited to be a 1.7-log increment from the original 2.5 logs for digital readout. In our design, FDG molecules depleted by the protein/enzyme complexes immobilized under a microwell can be replenished by the substrate diffusing in from the surrounding wells. Therefore, our analog ELISA method provides much higher substrate capacity for enzyme-based detection, conferring a broader dynamic range in comparison to Rissin' analog assay based on the isolated fL reactions, although the sensitivity is slightly compromised. Current microfluidic digital ELISA methods rely on manual, off-chip bead capture of targets followed by on-chip digital readout using fL compartments created by two-phase (oil/aqueous) isolation.[26,28] We envision that our microwell-based solid-phase ELISA technology provide an expandable platform for developing fully integrated microfluidic systems capable of performing automated ELISA in both digital and analog modes. We are currently working toward this goal in order to further improve the sensitivity, dynamic ranges, and reproducibility of proteomic analysis.

Conclusions

Here we have developed an integrated microfluidic system for rapid and ultrasensitive ELISA detection of protein biomarkers. In contrast to other existing microfluidic devices for solid-phase immunoassays, our system is able to perform flow-through immuno-capture in an open channel and subsequent chemifluorescence detection in a dramatically reduced volume, markedly improving the analytical sensitivity and speed. Using this novel method, we demonstrated the quantitative IGF-1R detection across five orders of magnitude with an extremely low detection limit of 3.5 fg mL^{-1} (21.8 aM), which substantially outperforms the commercial ELISA kits. Such improvement stems from the monolithic integration of a microvalve-based pump and the microwell-patterned assay chamber that can be pneumatically actuated. The ability of our assay to quantitatively detect protein biomarkers across a broad dynamic range will be beneficial for the clinical utilities as the target concentration can vary significantly in patients at different disease states. Moreover, the adaptation of the fL microwell pattern in our design opens opportunity to develop the next-generation microfluidic platforms that integrate and automate both digital and analog immunoassays to facilitate the advance of proteomics.

Acknowledgements

This work was supported by the new faculty start-up funds and the general research fund from the University of Kansas.

Notes and references

1 D. G. Spiller, C. D. Wood, D. A. Rand and M. R. White, *Nature*, 2010, **465**, 736–745.
2 M. Wu and A. K. Singh, *Curr. Opin. Biotechnol.*, 2012, **23**, 83–88.
3 Q. Shi, L. Qin, W. Wei, F. Geng, R. Fan, Y. S. Shin, D. Guo, L. Hood, P. S. Mischel and J. R. Heath, *Proc. Natl. Acad. Sci. U. S. A.*, 2012, **109**, 419–424.
4 D. G. Georganopoulou, L. Chang, J. M. Nam, C. S. Thaxton, E. J. Mufson, W. L. Klein and C. A. Mirkin, *Proc. Natl. Acad. Sci. U. S. A.*, 2005, **102**, 2273–2276.
5 P. R. Srinivas, B. S. Kramer and S. Srivastava, *Lancet Oncol.*, 2001, **2**, 698–704.
6 J. M. Nam, C. S. Thaxton and C. A. Mirkin, *Science*, 2003, **301**, 1884–1886.
7 M. Adler, R. Wacker and C. M. Niemeyer, *Analyst*, 2008, **133**, 702–718.
8 R. Malhotra, V. Patel, B. V. Chikkaveeraiah, B. S. Munge, S. C. Cheong, R. B. Zain, M. T. Abraham, D. K. Dey, J. S. Gutkind and J. F. Rusling, *Anal. Chem.*, 2012, **84**, 6249–6255.
9 K. N. Han, C. A. Li and G. H. Seong, *Annu Rev Anal Chem (Palo Alto Calif)*, 2013.
10 D. M. Rissin, C. W. Kan, T. G. Campbell, S. C. Howes, D. R. Fournier, L. Song, T. Piech, P. P. Patel, L. Chang, A. J. Rivnak, E. P. Ferrell, J. D. Randall, G. K. Provuncher, D. R. Walt and D. C. Duffy, *Nat. Biotechnol.*, 2010, **28**, 595–599.
11 A. M. Armani, R. P. Kulkarni, S. E. Fraser, R. C. Flagan and K. J. Vahala, *Science*, 2007, **317**, 783–787.
12 J. Kai, A. Puntambekar, N. Santiago, S. H. Lee, D. W. Sehy, V. Moore, J. Han and C. H. Ahn, *Lab Chip*, 2012, **12**, 4257–4262.
13 M. He and A. E. Herr, *J. Am. Chem. Soc.*, 2010, **132**, 2512–2513.
14 A. J. Rai, C. A. Gelfand, B. C. Haywood, D. J. Warunek, J. Yi, M. D. Schuchard, R. J. Mehigh, S. L. Cockrill, G. B. Scott, H. Tammen, P. Schulz-Knappe, D. W. Speicher, F. Vitzthum, B. B. Haab, G. Siest and D. W. Chan, *Proteomics*, 2005, **5**, 3262–3277.
15 Y. Zeng and T. Wang, *Anal. Bioanal. Chem.*, 2013, **405**, 5743–5758.
16 A. H. Ng, U. Uddayasankar and A. R. Wheeler, *Anal. Bioanal. Chem.*, 2010, **397**, 991–1007.
17 A. E. Herr, A. V. Hatch, D. J. Throckmorton, H. M. Tran, J. S. Brennan, W. V. Giannobile and A. K. Singh, *Proc. Natl. Acad. Sci. U. S. A.*, 2007, **104**, 5268–5273.
18 S. Numthuam, T. Ginoza, M. Zhu, H. Suzuki and J. Fukuda, *Analyst*, 2011, **136**, 456–458.
19 M. Herrmann, T. Veres and M. Tabrizian, *Lab Chip*, 2006, **6**, 555–560.
20 V. N. Morozov, S. Groves, M. J. Turell and C. Bailey, *J. Am. Chem. Soc.*, 2007, **129**, 12628–12629.
21 Y. Lu, J. J. Chen, L. Mu, Q. Xue, Y. Wu, P. H. Wu, J. Li, A. O. Vortmeyer, K. Miller-Jensen, D. Wirtz and R. Fan, *Anal. Chem.*, 2013, **85**, 2548–2556.
22 J. Kim, E. C. Jensen, M. Megens, B. Boser and R. A. Mathies, *Lab Chip*, 2011, **11**, 3106–3112.
23 C. T. Lim and Y. Zhang, *Biosens. Bioelectron.*, 2007, **22**, 1197–1204.

24 S. V. Pereira, J. Raba and G. A. Messina, *Anal. Bioanal. Chem.*, 2010, **386**, 2921–2927.
25 M. He and A. E. Herr, *Anal. Chem.*, 2009, **81**, 8177–8184.
26 C. W. Kan, A. J. Rivnak, T. G. Campbell, T. Piech, D. M. Rissin, M. Mosl, A. Peterca, H. P. Niederberger, K. A. Minnehan, P. P. Patel, E. P. Ferrell, R. E. Meyer, L. Chang, D. H. Wilson, D. R. Fournier and D. C. Duffy, *Lab Chip*, 2012, **12**, 977–985.
27 D. M. Rissin, D. R. Fournier, T. Piech, C. W. Kan, T. G. Campbell, L. Song, L. Chang, A. J. Rivnak, P. P. Patel, G. K. Provuncher, E. P. Ferrell, S. C. Howes, B. A. Pink, K. A. Minnehan, D. H. Wilson and D. C. Duffy, *Anal. Chem.*, 2011, **83**, 2279–2285.
28 S. H. Kim, S. Iwai, S. Araki, S. Sakakihara, R. Iino and H. Noji, *Lab Chip*, 2012, **12**, 4986–4991.
29 J. Todd, B. Freese, A. Lu, D. Held, J. Morey, R. Livingston and P. Goix, *Clin. Chem.*, 2007, **53**, 1990–1995.
30 D. A. Giljohann and C. A. Mirkin, *Nature*, 2009, **462**, 461–464.
31 X. Gao, L. Jiang, X. Su, J. Qin and B. Lin, *Electrophoresis*, 2009, **30**, 2481–2487.
32 X. Wang, X. Chen, X. Ma, X. Kong, Z. Xu and J. Wang, *Talanta*, 2011, **84**, 565–571.
33 O. Larsson, A. Girnita and L. Girnita, *Br J Cancer*, 2007, **96 Suppl**, R2–6.
34 J. E. Kucab and S. E. Dunn, *Breast Dis*, 2003, **17**, 41–47.
35 Y. Gong, E. Yao, R. Shen, A. Goel, M. Arcila, J. Teruya-Feldstein, M. F. Zakowski, S. Frankel, M. Peifer, R. K. Thomas, M. Ladanyi and W. Pao, *PLoS One*, 2009, **4**, e7273.
36 N. Peled, M. W. Wynes, N. Ikeda, T. Ohira, K. Yoshida, J. Qian, M. Ilouze, R. Brenner, Y. Kato, C. Mascaux and F. R. Hirsch, *Cell Oncol (Dordr)*, 2013.
37 S. J. Maerkl and S. R. Quake, *Science*, 2007, **315**, 233–237.
38 R. Fan, O. Vermesh, A. Srivastava, B. K. Yen, L. Qin, H. Ahmad, G. A. Kwong, C. C. Liu, J. Gould, L. Hood and J. R. Heath, *Nat. Biotechnol.*, 2008, **26**, 1373–1378.
39 Y. Zeng, R. Novak, J. Shuga, M. T. Smith and R. A. Mathies, *Anal. Chem.*, 2010, **82**, 3183–3190.
40 L. Yu, C. M. Li, Y. Liu, J. Gao, W. Wang and Y. Gan, *Lab Chip*, 2009, **9**, 1243–1247.
41 S. Lai, S. Wang, J. Luo, L. J. Lee, S. T. Yang and M. J. Madou, *Anal. Chem.*, 2004, **76**, 1832–1837.
42 N. Yanagisawa, J. O. Mecham, R. C. Corcoran and D. Dutta, *Anal. Bioanal. Chem.*, 2011, **401**, 1173–1181.
43 M. Herrmann, E. Roy, T. Veres and M. Tabrizian, *Lab Chip*, 2007, **7**, 1546–1552.
44 J. Park, V. Sunkara, T. H. Kim, H. Hwang and Y. K. Cho, *Anal. Chem.*, 2012, **84**, 2133–2140.
45 G. Proczek, A. L. Gassner, J. M. Busnel and H. H. Girault, *Anal. Bioanal. Chem.*, 2012, **402**, 2645–2653.
46 J. Kim, M. Kang, E. C. Jensen and R. A. Mathies, *Anal. Chem.*, 2012, **84**, 2067–2071.
47 D. M. Rissin, H. H. Gorris and D. R. Walt, *J. Am. Chem. Soc.*, 2008, **130**, 5349–5353.
48 Y. Zeng, M. Shin and T. Wang, *Lab Chip*, 2013, **13**, 267–273.
49 A. Lionello, J. Josserand, H. Jensen and H. H. Girault, *Lab Chip*, 2005, **5**, 1096–1103.
50 H. Parsa, C. D. Chin, P. Mongkolwisetwara, B. W. Lee, J. J. Wang and S. K. Sia, *Lab Chip*, 2008, **8**, 2062–2070.
51 E. C. Jensen, Y. Zeng, J. Kim and R. A. Mathies, *JALA*, 2010, **15**, 455–463.
52 G. Mountzios, I. Kostopoulos, V. Kotoula, I. Sfakianaki, E. Fountzilas, K. Markou, I. Karasmanis, S. Leva, N. Angouridakis, K. Vlachtsis, A. Nikolaou, I. Konstantinidis and G. Fountzilas, *PLoS One*, 2013, **8**, e54048.
53 J. M. Irish, N. Kotecha and G. P. Nolan, *Nat. Rev. Cancer*, 2006, **6**, 146–155.
54 L. Song, D. Shan, M. Zhao, B. A. Pink, K. A. Minnehan, L. York, M. Gardel, S. Sullivan, A. F. Phillips, R. B. Hayman, D. R. Walt and D. C. Duffy, *Anal. Chem.*, 2013, **85**, 1932–1939.
55 Y. Rondelez, G. Tresset, K. V. Tabata, H. Arata, H. Fujita, S. Takeuchi and H. Noji, *Nat. Biotechnol.*, 2005, **23**, 361–365.
56 Z. J. Huang, *Biochemistry*, 1991, **30**, 8535–8540.
57 N. Periasamy and A. S. Verkman, *Biophys. J.*, 1998, **75**, 557–567.
58 R. S. Gaster, D. A. Hall, C. H. Nielsen, S. J. Osterfeld, H. Yu, K. E. Mach, R. J. Wilson, B. Murmann, J. C. Liao, S. S. Gambhir and S. X. Wang, *Nat. Med.*, 2009, **15**, 1327–1332.